energies

MDPI

Article

Design and Sizing of Electric Bus Flash Charger Based on a Flywheel Energy Storage System: A Case Study

Mohammad Shadnam Zarbil [1], Abolfazl Vahedi [1,*], Hossein Azizi Moghaddam [2] and Pavel Aleksandrovich Khlyupin [3]

[1] Department of Electrical Engineering, Iran University of Science and Technology, Tehran 1684613114, Iran
[2] Electric Machines Research Group, Niroo Research Institute, Tehran 1468613113, Iran
[3] Department of Electrical Engineering and Electrical Facilities of Enterprises, Institute of Digital Systems, Automation and Energetics, Ufa State Petroleum Technological University, 450000 Ufa, Russia
* Correspondence: avahedi@iust.ac.ir

Abstract: At present, the trend of all sectors and industries, especially the oil and gas industry, is towards reducing carbon dioxide emissions. Along with the modernization of technological processes, special attention has been paid to the reduction in greenhouse gas emissions from vehicles that run on gasoline and diesel. An effective solution in this field is the transition from vehicles with combustion engines to electric vehicles, similar to the use of the electric bus in public transportation. How to charge these electric buses is a challenge for researchers. By proposing a flash charging method for electric buses, the feasibility of using these buses is obtained. Due to the pulsating nature of the power demand in this charging method, the prevention of negative effects on the network by this type of load should be considered. These negative effects can include power quality problems, voltage drop, frequency instability, and overload of transmission lines and transformers. This paper presents a flywheel energy storage system (FESS)-based flash charging station for electric buses. The specifications of the components of this charging station are designed and sized for a case study for line 1 of Tehran Bus Rapid Transit (BRT). A charging strategy based on the proposed charging cycle is presented to minimize the high-power short-duration demand from the grid. The energy consumption of the electric bus based on the electricity consumption model is calculated. Based on theoretical calculations, for the case study, there is a need for installing 12 flash charging stations based on FESS in line 1 Tehran BRT. In this line, an electric bus with a battery capacity of 80 kWh is proposed. The power and energy capacity of these charging stations are sized to 600 kW and 3.334 kWh, respectively. Additionally, an economic comparison regarding the proposed charging station is conducted. The theoretical results of the design and sizing of the proposed charging station are validated based on simulation and experimental results for a small-scale laboratory setup.

Keywords: carbon dioxide emissions; electric vehicle; electrification transportation; electric bus; flash charging technology; flywheel energy storage system

check for updates

Citation: Shadnam Zarbil, M.; Vahedi, A.; Azizi Moghaddam, H.; Khlyupin, P.A. Design and Sizing of Electric Bus Flash Charger Based on a Flywheel Energy Storage System: A Case Study. *Energies* **2022**, *15*, 8032. https://doi.org/10.3390/en15218032

Academic Editor: Amin Mahmoudi

Received: 6 October 2022
Accepted: 26 October 2022
Published: 28 October 2022

Publisher's Note: MDPI stays neutral with regard to jurisdictional claims in published maps and institutional affiliations.

Copyright: © 2022 by the authors. Licensee MDPI, Basel, Switzerland. This article is an open access article distributed under the terms and conditions of the Creative Commons Attribution (CC BY) license (https://creativecommons.org/licenses/by/4.0/).

1. Introduction

The transportation industry is one of the main contributors to the production and emission of carbon dioxide gas, including the transportation in the oil and gas industries, of which 60% is specialized transportation and 40% is technological transportation [1–3]. Therefore, the electrification of transportation has received more attention in recent years [4,5]. Many studies have been conducted regarding the effect of increasing the number of electric vehicles on the reduction in carbon emissions [6–8]. According to a study on the potential of the reduction in carbon dioxide emissions in German commercial transport by electric vehicles, the postal service can avoid CO2 emissions by about 40–70% if it uses "green" electricity for charging [7]. Additionally, based on the estimation of carbon dioxide emissions from the electrification of conventional diesel buses in Shenzhen, China, the use of

electric buses can reduce CO_2 emissions by 21.8% compared to conventional diesel buses in 2018 [8].

The fast-charging method is one of the attractive ways to enable the use of electric vehicles over long distances, which has a charging time of about a few minutes [9,10]. The charging power of the fast charger is in the range of 20 kW to 250 kW and more [11]. ABB has developed a 350 kW charger and claims it is the fastest charger available. The company has also developed and operated a 600 kW flash charger for TOSA electric buses [12,13]. As can be seen in Figure 1, the power of chargers has increased rapidly in recent years [13].

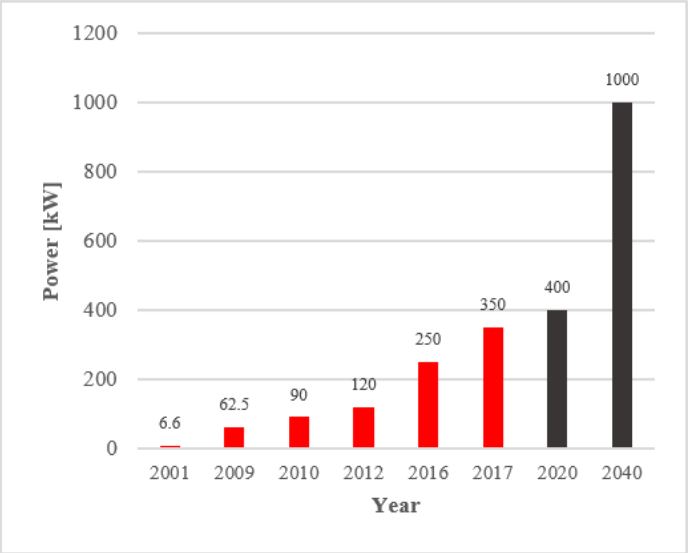


Figure 1. Increase peak power versus year for DC fast charger (red color for current power and gray color for predicted power) [13].

Based on the rate observed in Figure 1 and considering the expected development of battery technologies in the future, a peak power of 1 MW can be achieved in 2040. In this regard, the company "Trolleybus Optimisation System Alimentation (TOSA)" has built an electric bus route in Geneva, Switzerland, with the bus being charged in just 15 s at the station. This 15 s is the time required for passengers to get off and on the bus. When the bus stops at the station, a power of 600 kW is transmitted through a transmission device to the light batteries installed on the bus. The new technology, called "Flash Charging", was developed by engineers at ABB, one of the world's leading companies in power and automation technologies [12]. According to the World Bank report on air pollution in Tehran (health costs, resources, and policies) [14], mobile sources (vehicles) are the biggest cause of pollution in Tehran. According to Figure 2, 85% of pollution in Tehran is caused by heavy vehicles, among which the share of private sector buses is 35%, Tehran city buses is 28%, trucks is 28%, and minibuses is 8%.

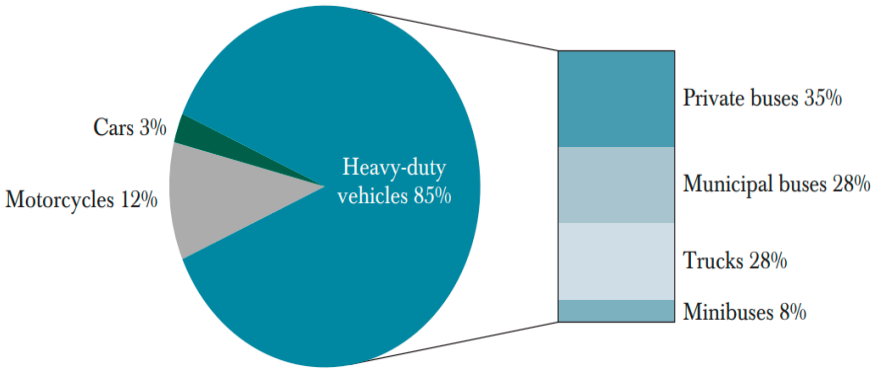


Figure 2. Mobile sources of pollution [14].

Therefore, the electrification of buses in Tehran is a of high priority. The TOSA flash charging solution enables the implementation of electric buses in the transportation fleet of Tehran. However, measures must be taken to supply the energy required by flash charging stations and to compensate for its negative effects. Flash charging technology is one of the ultra-fast chargering method that injects 600 kW into the E-bus battery in 15–20 s. It, therefore, imposes a "high peak short-term demand" on the power grid. This demand will have negative effects on the distribution network. So, a solution must be provided to eliminate or reduce these negative effects. One of the best solutions is using energy storage devices along with ultra-fast chargers. Due to the characteristics of flash charging technology, the desired storage device should have specifications such as fast response, high-power density, high efficiency, and high-duty cycle. In some studies, hybrid energy storage systems (HESS) have been used in electric vehicle charging stations. HESS is based on superconducting magnetic energy storage (SMES) and battery energy storage (BES) devices [15]. Additionally, FESS and BES storage units have been used in the application of charging stations based on renewable energy sources [16,17]. In the presented structures, Li-ion batteries, Ni-cd batteries, and lead-acid batteries are usually used for long-term energy supply. These batteries have some disadvantages, such as high cost, short life span, high maintenance costs, destructive impact on the environment, and a limited number of charges/discharges [18].

In this paper, a flywheel energy storage system (FESS)-based electric bus charging station for a case study in Tehran BRT is presented. According to the specifications of the chosen Tehran BRT line, the power and energy requirements for the charging station are obtained in such a way that it has the least negative impact on the power grid. In Section 2, a topology for the E-bus charging station is proposed and the technical specification of each charging station is obtained. In Section 3, an economic calculation was conducted in order to compare the cost of using FESS instead of lead-acid battery in the charging station. In Section 4, a control method for FESS is described. In Section 5, the proposed charging station is simulated and the calculated specifications are compared with the simulation results. In Section 6, a downsized laboratory setup for the proposed charging station is implemented and the experimental results are compared with the simulation and calculated results. Finally, in Section 7, the conclusion of the results for the proposed charging station is presented.

2. Proposed E-Bus Flash Charging Design and Sizing

To size a FESS-based flash charging station, the first step is choosing a bus route in the city. For this purpose, Line 1 of Tehran BRT was selected. The specifications of this bus line are shown in Table 1.

Table 1. The specification of line 1 of Tehran BRT.

Specification	Value
Number of stations	31
Distance	18.7 km
Duration along the way	45 min
Start time	5:03 AM
End time	9:55 PM

According to the start and end time of Line 1 of Tehran BRT, the travel time of buses on the route is 16 h and 52 min. As a result, depending on the length of the journey, the number of times (N_b) that a bus travels between the start and end of the line can be calculated as follows:

$$N_b = \frac{1012 \text{ min}}{45 \text{ min}} \approx 23 \quad (1)$$

Based on the schedule of buses according to the Website of Tehran Bus Company, the minimum travel time from one station to another is 2 min. Additionally, the average stop time of each bus at the station is 30 s. To equip this expressway with an electric bus, the TOSA electric bus shown in Figure 3 was used [8]. This bus has two battery packs, each with a capacity of 40 kWh. As a result, the total battery capacity of the TOSA bus is $E_b = 80$ kWh [11]. This bus is charged with a pantograph that can be disconnected and reconnected in a short time (less than 5 s).



Figure 3. TOSA electric bus.

For remaining the bus on the line 1 route, the remaining capacity of the bus battery, taking into account the minimum state of charge $SOC_{b,\min} = 30\%$, must be as follows:

$$E_{b,res} = 30\% \times 80 \text{ kWh} = 24 \text{ kWh} \quad (2)$$

The energy consumption of the TOSA electric bus by the implementation of the electricity consumption model (ECONS-M) [19,20] and using TOSA electric bus specifications [21] was obtained. This model calculates the longitudinal dynamics of the vehicle as a function of the speed of the driving cycle. The main output of this model is the characteristic of electric bus energy consumption. For a vehicle in motion, the traction force can be obtained using a simple two-dimensional application of Newton's second law to describe the translational and rotational systems. Newton's second law is expressed as follows:

$$M \times \vec{a} = \sum \vec{F} \quad (3)$$

where M, a, and F are mass of an object, acceleration, and force, respectively. In this model, the effect of angular moments created by rotating propulsion components was obtained by adding an equivalent mass (M_{equ}) to the vehicle mass, according to Equations (3)–(6). This mass is estimated to be 10% of the vehicle weight for buses [22]. Figure 4 shows the free-body diagram of a moving vehicle. The main forces acting on the body are the grade force (F_g), the rolling resistance force (F_r), and the aerodynamic force (F_a).

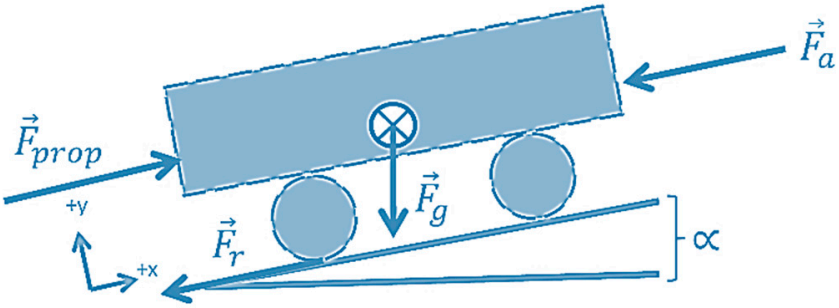


Figure 4. Free body diagram of the bus in motion.

The F_{prop} represents the force provided by the motor to propel the vehicle by overcoming external resistance forces. Based on this, Equation (3) can be rewritten as follows:

$$(M + M_{equ})a(t) = F_{prop}(t) - F_{tot}(t) \tag{4}$$

where F_{tot} is the sum of the external forces acting on the vehicle. The grade force (F_g), aerodynamic force (F_a), and rolling resistance force (F_r) are, respectively, defined in the following equations.

$$F_g(t) = (M + M_{eq}) \times g \times \cos(\alpha) \tag{5}$$

$$F_a(t) = \frac{1}{2} \times \rho \times A \times C_D \times V(t)^2 \tag{6}$$

$$F_r(t) = C_r(V\ (t)) \times (M + M_{eq}) \times g \times \sin(\alpha) \tag{7}$$

In Equation (5), α is the slope of the road in degrees and g is the standard gravity constant. In Equation (6), ρ is the air density, A is the front cross-section of the car, C_D is the drag coefficient, and V is the car speed. Finally, in Equation (7), C_r is the rolling resistance coefficient, which depends on the vehicle speed and the condition of the tires. The rolling resistance coefficient is obtained from the following equation.

$$C_r(V\ (t)) = 0.006 + 4.5 \times 10^7 \times V\ (t)^2 \tag{8}$$

By obtaining $F_{prop}(t)$ from Equation (4), the wheel torque $T_W(t)$ is obtained using the following equation:

$$T_W(t) = F_{prop}(t) \times R_w \tag{9}$$

In the above relationship, R_w is the radius of the wheel. The electric motor torque T_M is related to wheel torque according to the following relationship.

$$T_M(t) = \frac{T_W(t)}{GR \times \eta_T} \tag{10}$$

where GR is the ratio constant of the bus gearbox and η_T is the transmission efficiency constant.

The rotational speed $\omega_W(t)$ of the wheels is obtained from the following equation:

$$\omega_W(t) = \frac{V(t)}{R_W} \tag{11}$$

The relationship between wheel rotational speed and motor rotation speed is as follows:

$$\omega_M(t) = \omega_W(t)\ \times\ GR \tag{12}$$

With the motor efficiency available (η_M), the instantaneous power consumption of the bus is obtained from the following relationship:

$$P_{inst}(t) = P_{cons}(t) = \frac{T_M(t) \times \omega_M(t)}{\eta_M \times \eta_{conv}} + \frac{P_{auxi}}{\eta_{conv}} \tag{13}$$

In the above relationship, η_{conv} is the efficiency of the converter and P_{auxi} is the required power of the peripheral equipment.

When the bus brakes, the motor turns into a generator. This allows the partial recovery of kinetic energy to recharge the batteries. In the case of regeneration, the instantaneous power is:

$$P_{elec,batttery} = T_{M,reg}(t) \times \omega_M(t) \times \eta_{M,reg}\ \times\ \eta_{conv}\ + \frac{P_{auxi}}{\eta_{conv}} \tag{14}$$

In the above relation, $T_{M,reg}$ is the motor torque when the bus uses regenerative braking. Finally, the energy consumption of the electric bus is obtained simply by integrating the instantaneous power in terms of time in the form of the following relationship:

$$E_{total} = \int_0^{t_{end}} P_{inst}(t)\, dt \tag{15}$$

The main application of this model is to determine the total energy extracted or supplied from the battery to power the bus under certain driving conditions. The approach described in this analysis is a systematic approach for which the main propulsion components are represented by functions that can be fixed or changed according to different parameters (such as torque, speed, and temperature). The system used to model electric bus energy consumption is shown in Figure 5. To calculate the energy consumption of the electric bus according to the proposed energy consumption model, the input parameters are presented in Table 2.

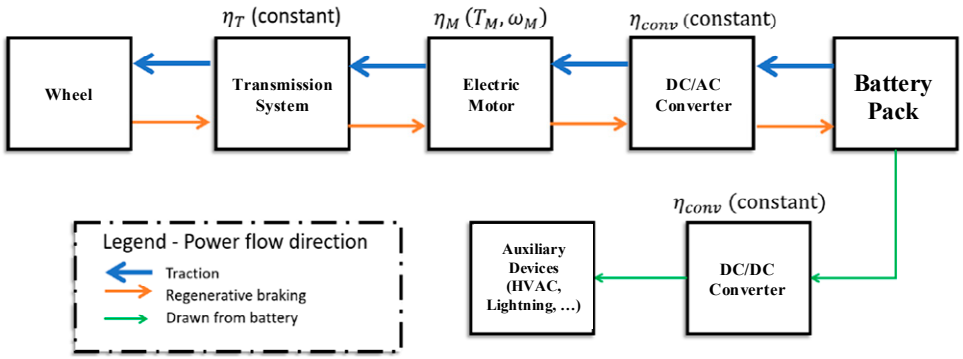


Figure 5. Electric bus energy consumption model system components.

Table 2. Input parameters to obtain the electric bus energy consumption model.

Parameter	Unit	Value
Bus Physical Characteristics		
Weight	kg	16,914
Front cross-section	m^2	8.66
Number of passengers	-	37
Wheel radius	m	0.5
Performance Specifications of Electric Motor		
Gear ratio	-	15
Transmission system efficiency (engine to wheels)	-	95%
Converter efficiency	-	97%
Power sharing ratio of regenerative brakes	-	40%
Battery capacity	kWh	80
Environmental Characteristics		
Air density	kg/m^3	1.225
Drag coefficient	-	0.6
Rolling resistance coefficient	-	0.01

By substituting the parameters presented in Table 2 and considering an auxiliary devices power equal to 2.5 kW (heating, ventilation, and air conditioning (HVAC) in on), the average energy consumption of the electric bus is:

$$TOSAenergy\ consumption = 1.05\ \ ^{kWh}/_{km} \tag{16}$$

As a result, the total energy consumption of the bus during the journey from the beginning to the end of Line 1 is obtained from the following equation:

$$E_{consumption} = 18.7\ km\ \times\ 1.05\ ^{kWh}/_{km}\ =\ 19.635\ kWh \tag{17}$$

According to (2), the allowable amount of energy consumption from the initial capacity of the battery in each path is obtained from the following equation:

$$\begin{aligned} E_{b_1trip_consumption} &= \frac{\left(1-\left(SOC_{b,\min}\right)\right)E_b}{N_b} \\ &= \frac{(1-0.3)\times 80 \text{ kWh}}{23} = 2.43 \text{ kWh} \end{aligned} \tag{18}$$

According to Equations (17) and (18), the capacity required to charge the bus battery along the route from beginning to end is obtained from the following equation:

$$\begin{aligned} E_{t,charge} &= E_{consumption} - E_{b_1trip_consumption} \\ &= 19.635 - 2.43 \ = 17.205 \text{ kWh} \end{aligned} \tag{19}$$

By selecting 6 stations on the way and 6 stations on the return route as FESS-based flash charging stations (a total of 12 stations along Tehran line 1 BRT), the minimum amount of charging energy of each charging station is obtained from the following equation:

$$E_{charge} = \frac{E_{t,charge}}{6} \ = 2.867 \text{ kWh} \tag{20}$$

Therefore, each FESS-based flash charging station should charge the electric bus battery with a minimum energy of $E_{\text{charge}h} = 2.867$ kWh. Since the electric bus stops at the station for $\Delta t_{ch} = 20$ s, during this time the charging station with a power of 600 kW charges the bus battery. Therefore, the charging capacity is obtained from the following equation, which must be greater than the minimum energy required to charge the electric bus:

$$E_{ch} = P_{ch} \times \Delta t_{ch} \ = 600 \text{ kW} \ \times \ 20 \text{ s} \ = 3.334 \text{ kWh} \geq 2.867 \text{ kWh} \tag{21}$$

2.1. Energy Storage Device Selection

Given that, all the energy to charge the battery of the electric bus must be provided by the FESS, a flywheel system with a capacity higher than this charging capacity must be selected. Therefore, two paralleled flywheel systems, as shown in Figure 6, were selected. The total capacity of FESS for the charging station was selected as follows:

$$E_F \ = E_{F1} + E_{F2} = 3.47 \text{ kWh} \tag{22}$$

$$P_F \ = P_{F1} + P_{F2} = 600 \ \text{kW} \tag{23}$$

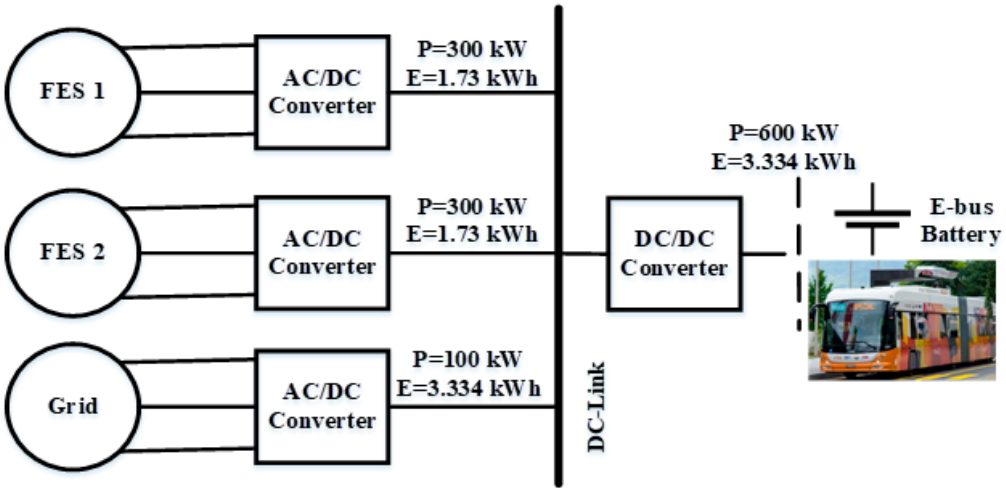


Figure 6. Proposed electric bus flash charging station.

The torque-speed characteristic of the FESS electric machine includes two values of continuous torque (rated) and transient torque (peak). Therefore, the electric machine can provide, for example, 30 s of peak torque up to 100% of the rated torque at the charging and discharging mode. In this case, it can be assumed that the power in the short time of 20 s during E-bus charging is constant.

2.2. FESS Recharging Power and Energy Design

According to the required charging capacity, the discharge capacity of each flywheel during the charging period of the electric bus at the station is obtained from the following relation:

$$E_{dch,F1} = E_{dch,F2} = \frac{E_{ch}}{2} = 1.665 \text{ kWh} \tag{24}$$

Given the minimum travel time from one station to another by bus, the maximum time to recharge the flywheel over the network is as follows:

$$\Delta t_{rch,\ max} = 2 \text{ min} \tag{25}$$

According to Equations (11) and (12) and assuming that the flywheels are recharged to the same extent as their discharge capacity in the bus battery, the power of the power grid to charge the first flywheel system is obtained as follows:

$$P_{G1} \times \Delta t_{rch,max} = E_{dch,F1} \Rightarrow P_{G1} = \frac{1.665 \text{ kWh}}{2/60 \text{ h}} = 50 \text{ kW} \tag{26}$$

The power required to recharge the second flywheel system is the same as the first flywheel system. As a result, the total network power is as follows:

$$P_G = P_{G1} + P_{G2} = 100 \text{ kW} \tag{27}$$

The power circuit of the electric bus charging station is shown in Figure 6. The station includes two FESS, power grid, and a flash charger. The electric bus is charged at the station with a power capacity of 600 kW and energy capacity of 3.33 kWh, which is supplied through two parallel flywheel systems. When there are no buses at the station, two parallel flywheels are recharged through a power of 100 kW grid with an energy capacity of 3.33 kWh.

The duty cycle of the flash charging station is shown in Figure 7. Additionally, the proposed structure is shown in Figure 8. Since the electric bus arrives at the station, the pantograph is connected to the battery from the top of the bus for a maximum time of $\Delta t_C = 5$ s. The bus battery is then charged for a maximum time of $\Delta t_{Ch} = 20$ s. During this time, two parallel flywheel systems are discharged to the bus battery. After disconnecting the pantograph, which takes the maximum time of $\Delta t_d = 5$ s, the phase of recharging the flywheel systems through the power grid begins at the maximum time of $\Delta t_{rch} = 2$ min. This cycle is repeated when the next bus arrives. Based on the charging duty cycle, the flowchart of the charging strategy is shown in Figure 9.

According to Equation (24) the maximum FESS energy is available. According to the converter efficiency of the FESS system, the following result is obtained:

$$\eta_{Inv.} = \frac{E_{FES,out}}{E_{FES,in}} \Leftrightarrow E_{FES,in} = \frac{1.736 \text{ kWh}}{0.9} = 1.928 \text{ kWh} \tag{28}$$

By obtaining FESS energy, other parameters can be designed. The energy of the flywheel system is as follows:

$$E_{FES,in} = \frac{1}{2} J\omega^2 \tag{29}$$

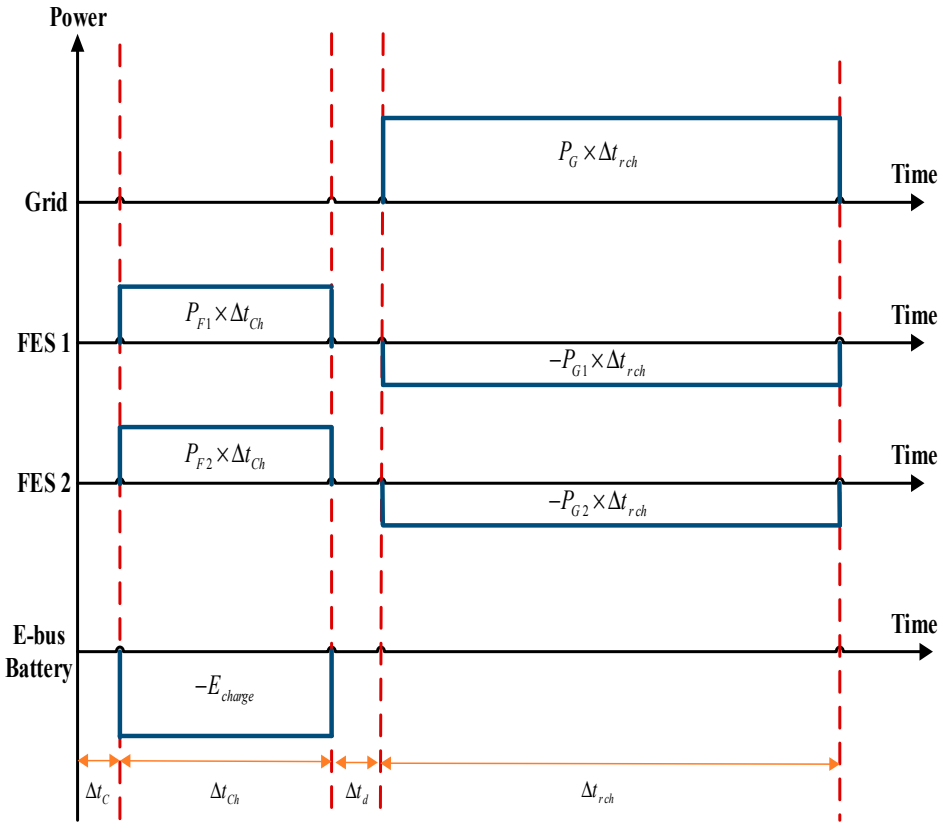


Figure 7. Proposed flash charging duty cycle.

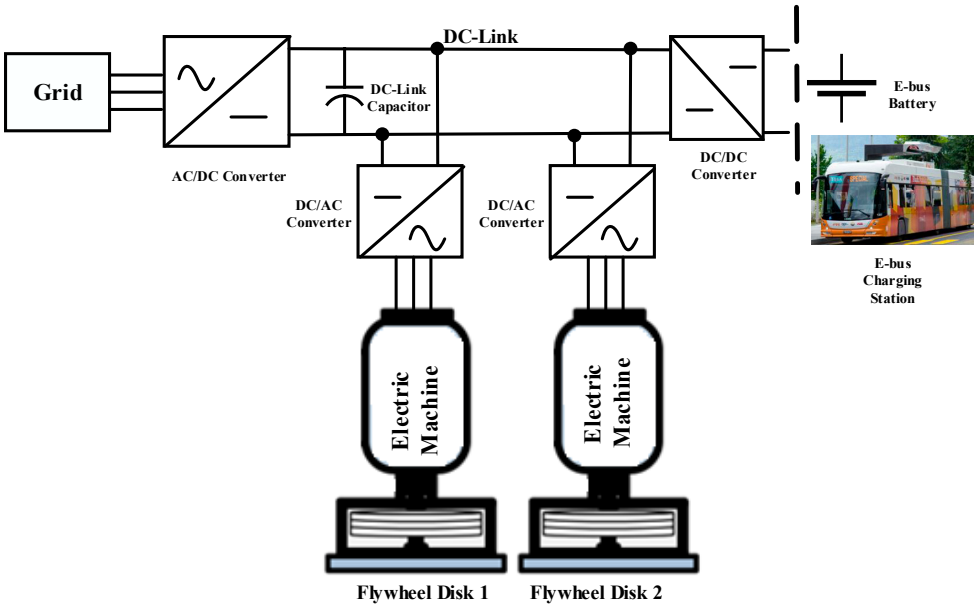


Figure 8. Proposed E-bus flash charging structure.

In the above relation, J is the moment of inertia of the flywheel disk and ω is the rotation angular velocity of the flywheel. For design for the desired speed of 14,000 rpm the rotation angular velocity of FESS is obtained as follows:

$$\omega = \frac{2\pi}{60} N_{rpm} = \frac{2\pi}{60} \times 14,000 = 1466 \text{ rad/s} \quad (30)$$

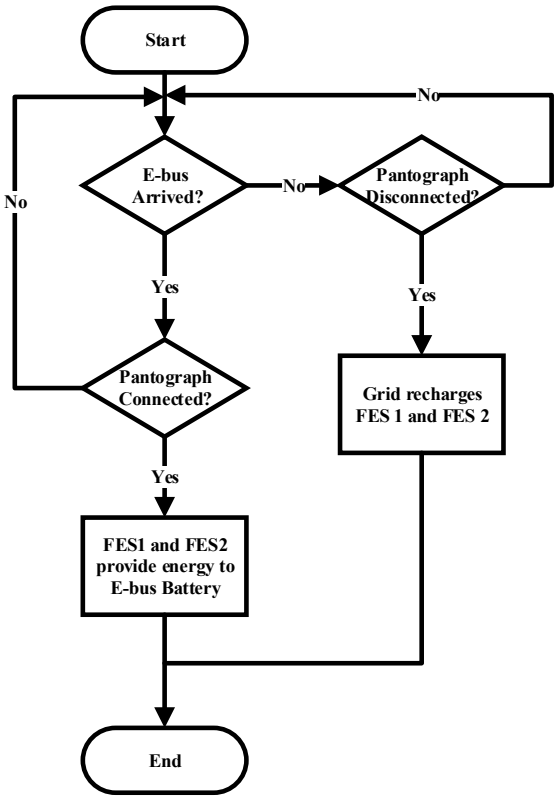


Figure 9. Proposed station charging strategy flowchart.

The moment of inertia of the flywheel is achieved as follows:

$$J = \frac{2 \times E_{FES,in}}{\omega^2} = \frac{2 \times 1.928 \times 3600 \times 10^3}{1466^2} \approx 6.5 \text{ kg·m}^2 \tag{31}$$

The moment of inertia equation can be defined as follows:

$$J = m \times r^2 \tag{32}$$

where m is the mass of the flywheel disk in kilograms (kg) and r is the radius of the disk in meters (m). Given that, the moment of inertia is obtained from Equation (18) and assuming $m = 50$ kg, the flywheel radius is obtained from the following equation:

$$r = \sqrt{\frac{J}{m}} = \sqrt{\frac{6.5 \text{ kg·m}^2}{50 \text{ kg}}} = 0.36 \text{ m} = 36 \text{ cm} \tag{33}$$

Depending on the application, different geometric structures with different types of materials, such as steel, composite, and nanotechnology, are provided for the flywheel, each of which has different mechanical stress [23,24]. The geometric structure of the FESS is shown in Figure 10. In this structure, the flywheel disc is connected to the rotor part through a mechanical coupling. Table 3 shows the geometrical dimensions of the flywheel disk. Based on the designed flywheel disk, the maximum mechanical stress in terms of the outer radius and the maximum speed of the flywheel disc is shown in Figure 11. As can be seen, with the increase in the outer radius and speed of the flywheel, the mechanical stress increases significantly. At the maximum speed of 14,000 rpm and the outer radius of 15 cm, the amount of stress increases to about 220 Mpa. According to the calculation results, in the worst working conditions, the maximum stress is lower than the allowed value for steel material (250 Mpa).

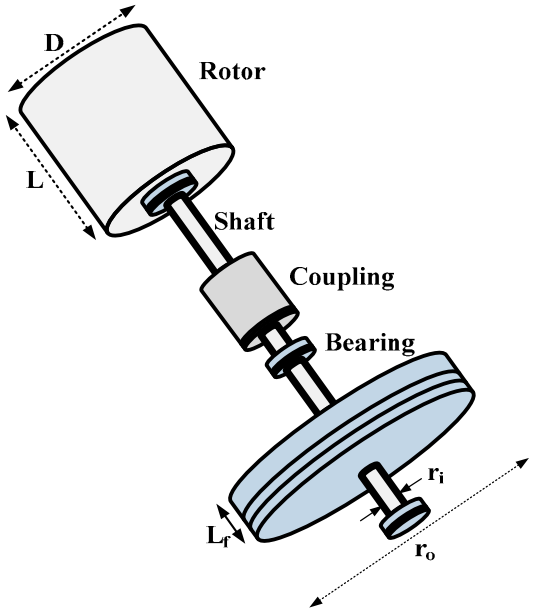


Figure 10. The geometrical structure of FESS.

Table 3. The geometrical dimensions of the designed flywheel disk.

Diomension	Value
r_{omax}(cm)	35.77
V_{max}(m/s)	340
r_i(cm)	2
r_o(cm)	15
L_f(cm)	3.5

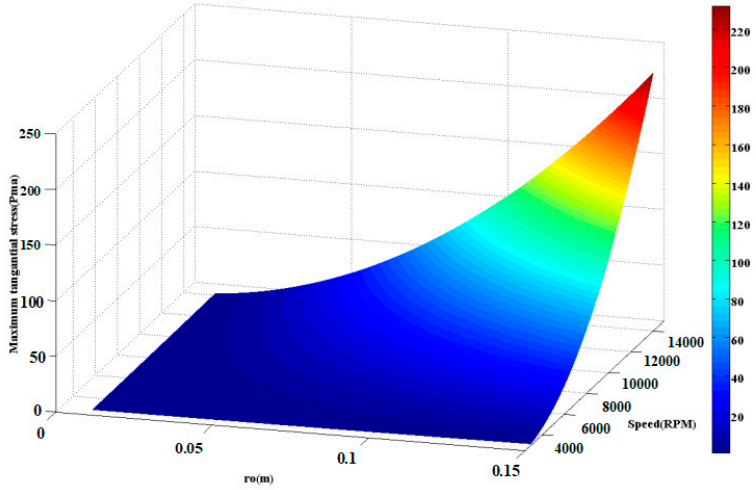


Figure 11. The maximum mechanical stress of the flywheel disk.

2.3. Power Electronics Converter Design

According to the proposed structure for the charging station, through an ac/dc converter (three-phase rectifier), power flows from the grid to the dc-link. Additionally, through a bidirectional dc/ac converter (three-phase inverter), power and energy flows from the FESS to the dc-link and vice versa. In this section, the technical specifications of these two power electronics converters is obtained. The structure of the grid-side converter is shown in Figure 12.

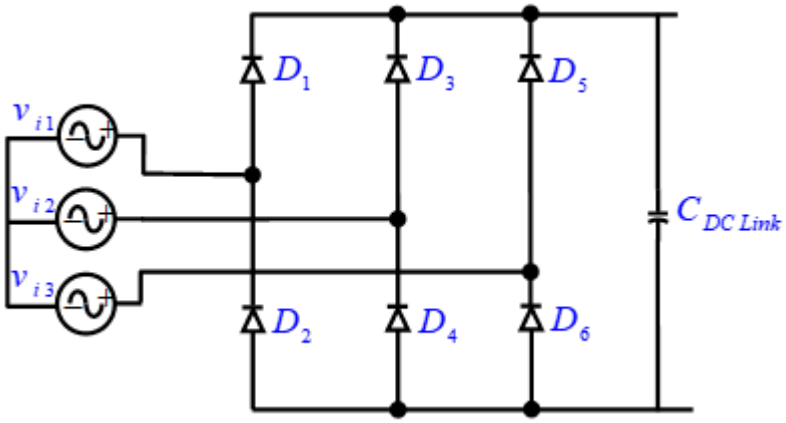


Figure 12. Grid side converter of the fast-charging station.

According to grid power to charge FESS, the dc-link current is obtained as follows:

$$I_{G_DC} = \frac{P_G}{V_{DC}} = \frac{100\ \text{kW}}{600} = 166.67\ \text{A} \tag{34}$$

Assuming the rectifier converter efficiency is equal to $\eta_{Rec.} = 0.9$ and the design for DC output power from the grid is equal to P_G, the following equation for the AC power required from the network (P_{G_AC}) is obtained.

$$\eta_{Rec.} = \frac{P_G}{P_{G_AC}} \Leftrightarrow P_{G_AC} = \frac{100\ \text{kW}}{0.9} = 111.11\ \text{kW} \tag{35}$$

For a power factor ($PF = 0.8$) for the grid, the RMS value of the grid current ($I_{G,rms}$) is obtained from the following equation:

$$I_{G,rms} = \frac{P_{G_AC}}{3 \times V_{G,rms} \times PF} = \frac{111.11\ \text{kW}}{3 \times 220 \times 0.8} = 210.4\ \text{A} \tag{36}$$

During FESS charging mode, energy is transferred from the dc-link to the machine (motor operation) and during discharging mode, energy is transferred from the flywheel to the dc-link (generator operation). The structure of the FESS converter is shown in Figure 13.

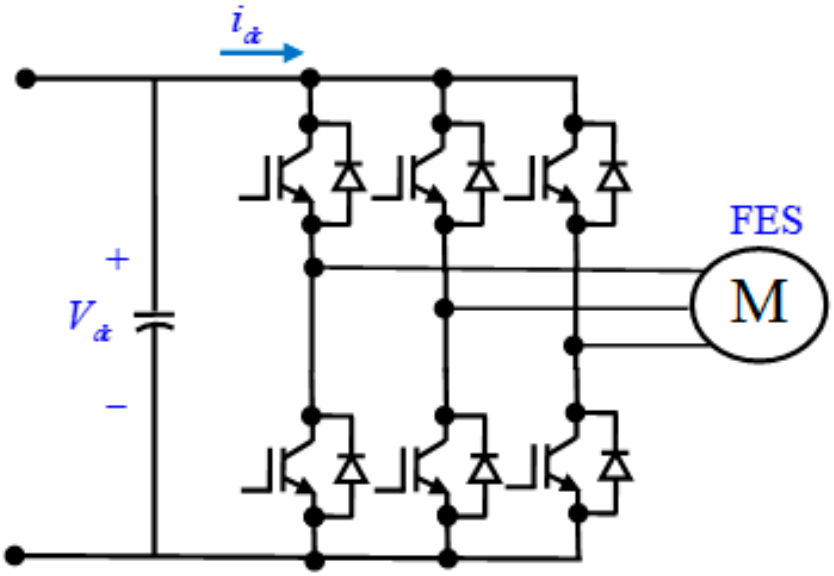


Figure 13. Flywheel system converter.

The FESS is designed to provide a maximum output power equal to the power of the charging station (P_{DC}). Given that the DC bus voltage is constant, the DC bus current can be calculated as follows:

$$I_{F_DC} = \frac{P_{F_DC}}{V_{DC}} = \frac{600\ \text{kW}}{600} = 1000\ \text{A} \tag{37}$$

According to the use of two FESS as parallel to provide power derived by the charger, the following results are obtained:

$$\begin{array}{l} I_{F1_DC} = I_{F2_DC} = 500\ \text{A} \\ P_{F1_DC} = P_{F2_DC} = 300\ \text{kW} \end{array} \tag{38}$$

Assuming the converter efficiency equal to $\eta_{Inv.} = 0.9$, the AC power of the electric machine is obtained from the following equation:

$$P_{F_AC} = \frac{P_{F1_DC}}{\eta_{Inv.}} = \frac{300\ \text{kW}}{0.9} = 333.33\ \text{kW} \tag{39}$$

FESS generally has two key characteristics, which include power capacity and energy capacity. The power capacity depends on the design of the machine and power electronic converters, such as the current density of the stator winding, the cooling system, and the rating of the power electronic converters and their cooling system. Therefore, the peak charging and discharging power of the FESS can be achieved by selecting the power capacity of the electric motor and interface converters for different values. Another parameter is the energy capacity of the FESS, which depends on the inertia of the rotating disk and the speed of the storage device. Since, according to Equation (16), the value of energy is related to the square of the speed, high-speed flywheels are used for applications that require high energy capacity. However, in applications that require very high-power capacity and long storage time (similar to series or parallel batteries), it is possible to combine small flywheel storage units and achieve high-power and -energy capacities.

By entering a pulsed load (electrical bus load) during charging (energy change) according to Equation (40), it causes a change in the speed of the flywheel disc. In the charging mode of the electric bus, the speed of the flywheel is decreased, which depends on the charging time (t_{int}), charging power (P_{load}), charging FESS efficiency (η_f), and disk inertia (J). When recharging the flywheel, the speed of the flywheel increases similarly.

$$\Delta\omega^2 = \omega_o^2 - \omega_{\text{min}}^2 = \frac{2}{J}\frac{P_{load}\ t_{\text{int}}}{\eta_f} \tag{40}$$

3. Economic Comparison

In this paper, the flywheel energy storage device was used in the electric bus flash charging station instead of the lead-acid battery storage device. So, an economic comparison was made between these two storage devices. In general, there are two methods of total capital cost (TCC) and life cycle cost (LCC) for cost calculation [25]. The main cost items of FESS and the lead-acid battery are stated in Table 4.

According to the values of the main costs for FESS and lead-acid battery presented in Table 4 and the calculation equations of the levelized cost of electricity (LCOE), the annualized life cycle costs (ALCC) and the total capital cost (TCC), the results are provided in Table 5 [25]. According to the results presented in this table, FESS has a lower cost in all three mentioned costs compared to the lead-acid battery. Therefore, the flash charging station based on FESS presented in this paper is economically better than the conventional charging stations based on lead-acid battery.

Table 4. Main cost items of FESS and lead-acid batteries [25].

Cost Item	Average	Range
Flywheel Energy Storage System		
Power Conversion System [a] (PCS) (EUR/kW)	287	263–470
Storage Section [b] (EUR/kWh)	2815	865–47,764
Fixed Operational and Maintenance (EUR/kW-y)	5.2	4.3–6
Variable Operational and Maintenance (EUR/kWh)	2	0.2–3.8
Replacement [c] (EUR/kWh)	151	85–216
Lead-Acid Battery		
Power Conversion System (EUR/kW)	378	195–594
Balance of Plant (BOP) (EUR/kW)	87	43–130
Storage Section [d] (EUR/kWh)	618	184–847
Fixed Operational and Maintenance (EUR/kW-y)	3.4	3.2–13
Variable Operational and Maintenance (EUR/kWh)	0.37	0.15–0.52
Replacement [e] (EUR/kWh)	172	50–560

[a] Including BOP costs. [b] As flywheel systems are typically employed for power quality applications with discharge time of seconds up to 30 min, the direct use of storage cost may entail ambiguity. [c] Every four years, given based on the unit of power rating. [d] Mainly for MW-scale systems with rated DoD of 80%, used for bulk energy storage and T&D support (discharge time 4 h). [e] Every 8 y for the mentioned application (365 cycles per year).

Table 5. Cost comparison for FESS and lead-acid battery.

Cost Index	FESS	Lead-Acid Battery
Levelized Cost of Electricity (LCOE) (EUR/kWh)	0.1983	0.225
Annualized Life Cycle Costs (ALCC) (EUR/kW-y)	495.77	580
Total Capital Cost (TCC) (EUR/kW) (EUR/kWh)	377	2400

4. FESS Control Method

In this section, to control the FESS, the maximum torque per ampere (MTPA) control system was used. The block diagram of this control system is shown in Figure 14. In this figure, I_{ds} and I_{qs} are the stator d-axis and q-axis currents, respectively. Additionally, V_d and V_q are the d and q axes voltages are generated for controlling the system, respectively [26]. The rotor position (θ) is used in qd to abc transformation. This method of control has two internal controllers to control the current and an external control loop to control the supply power, which is called a cascade controller [27,28]. In this control method, to calculate the reference currents of the d and q axes, it is necessary to calculate the optimal angle of the phase current (β). This optimal angle is calculated as follows [29]:

$$\beta = \sin^{-1}\left(\frac{-\lambda + \sqrt{\lambda^2 + 8\left(L_{ds} - L_{qs}\right)^2 {I_s}^2}}{4\left(L_{ds} - L_{qs}\right) I_s}\right) \tag{41}$$

where I_s is obtained from the outer loop controller. With consideration β, reference currents of the d and q axes can be calculated as follows:

$$I_d{}^* = I_s \cos(\beta) \tag{42}$$

$$I_q{}^* = I_s \sin(\beta) \tag{43}$$

In the outer loop, by holding the dc bus voltage constant, the reference power of the flywheel is obtained, which must be supplied by two parallel flywheels.

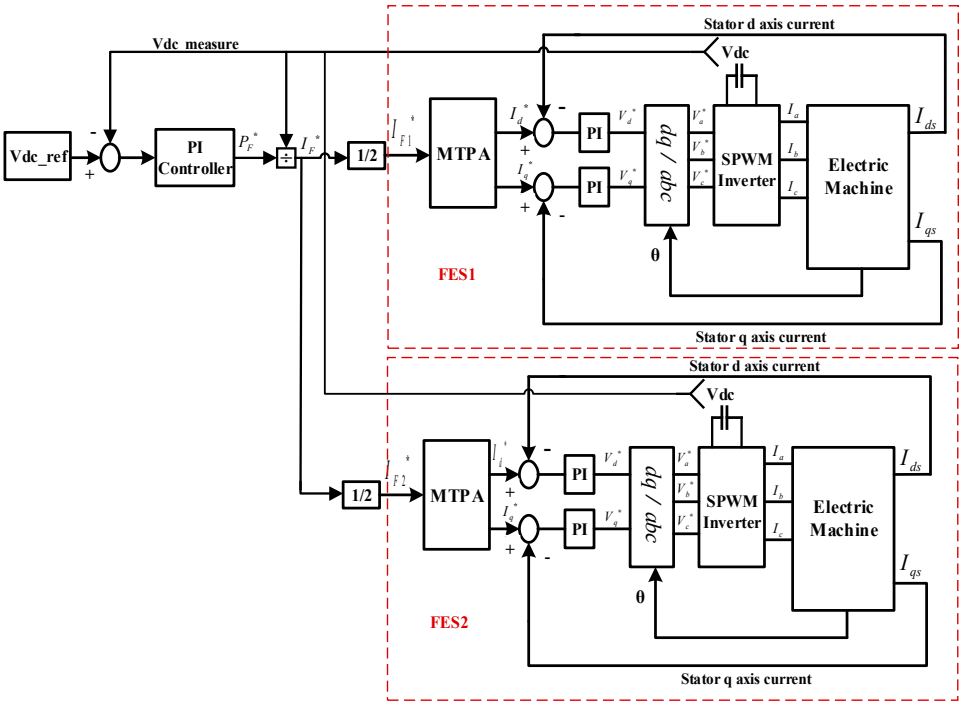


Figure 14. FESS control block diagram.

5. Simulation Results

The proposed structure of the flywheel-based flash charging station, shown in Figure 8, was simulated with the electric bus charging cycle following Figure 7. To control two parallel flywheels, the control method presented in Figure 14 was used. The simulation results for electrical power are shown in Figure 15. According to this figure, in this simulation, an electric bus enters the station at $t = 0$ s. At $t = 5$ s, the power transmission system (pantograph) is connected to the electric bus and is ready to charge the battery of the electric bus for $\Delta t_{ch} = 20$ s. During this time, the $P_{ch} = 600$ kW electric bus battery, all powered by two parallel flywheels, is charged. The charging power is evenly divided between the two flywheels according to the control method, and each has the task of supplying $P_{F1} = P_{F2} = 300$ kW power. After the power transmission system (pantograph) is completely disconnected from the electric bus, which takes $t = 5$ s, both flywheels with a power of $P_{F1} = P_{F2} = 50$ kW each, the total of which is supplied from the network, are recharged for $\Delta t_{rch} = 120$ s. The next cycle is repeated exactly as the next bus arrives. Figure 16 shows the DC currents drawn from the mains and flywheels and the injected currents from the charger to the battery of the electric bus. Given that the DC bus voltage is $V_{DC} = 600$ V (as shown in Figure 17), the values of the currents are obtained by dividing the electric power by the DC bus voltage. As can be seen from Figure 17, at the time of disconnection and connection of energy sources, the voltage fluctuates, which according to the proposed control method (Figure 14) this oscillation is the criterion for generating compensating power through flywheels. Figure 18 shows the energy of each power source and charger. As can be seen from this figure, at the time of battery charging, each flywheel is discharged at a rate of $E_{dch,F1} = E_{dch,F2} = 1.665$ kWh, which is per Equation (11). Additionally, when charging, the charger charges the electric bus battery at $E_{ch} = 3.336$ kWh according to (8). While waiting for the charging station, two flywheels are recharged through the mains at the same discharge capacity.

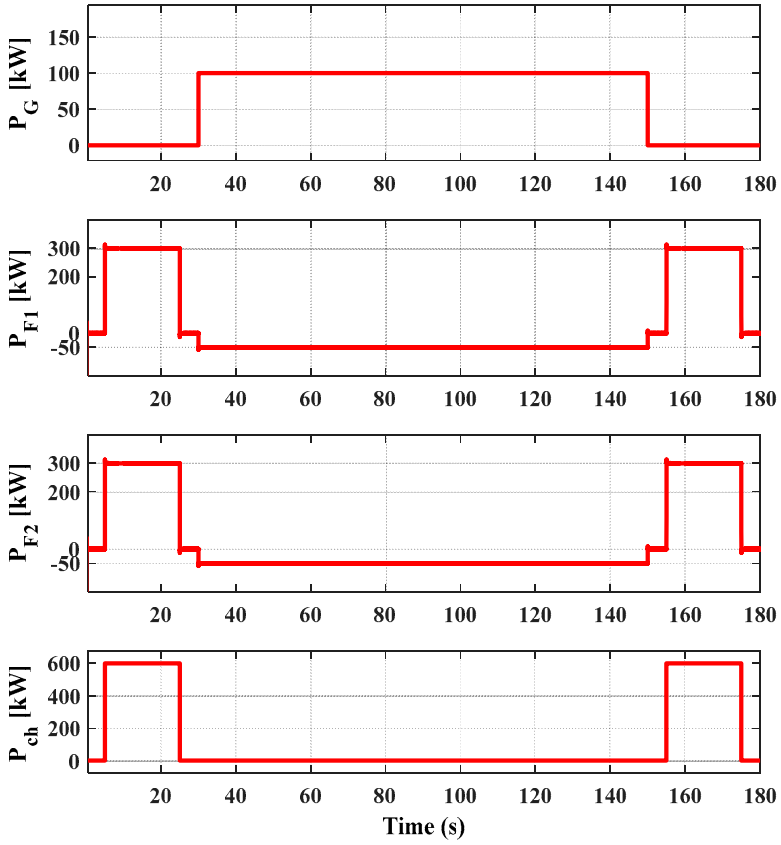


Figure 15. Simulation results for the electric power of grid, FES1, FES2, and charger.

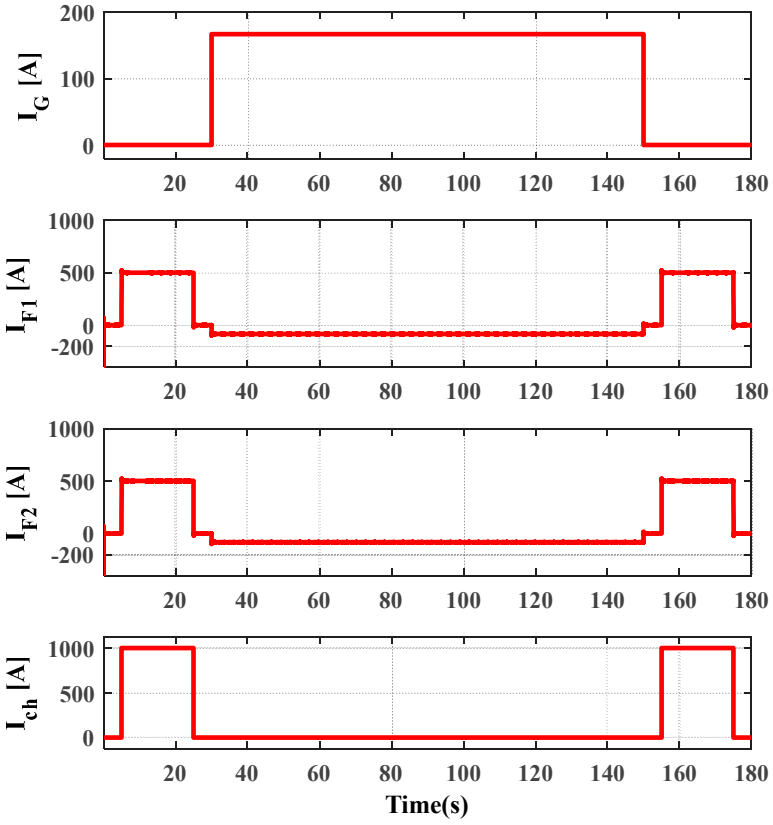


Figure 16. Simulation results for the electric current of the grid, FES1, FES2, and charger.

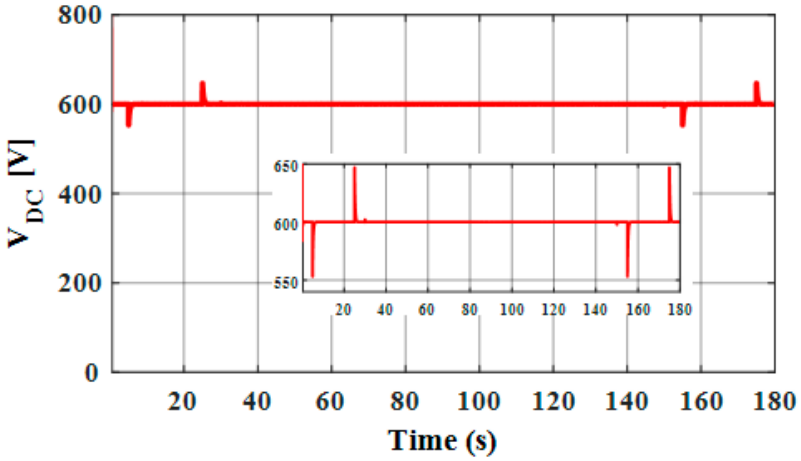


Figure 17. Simulation results for the DC-link voltage.

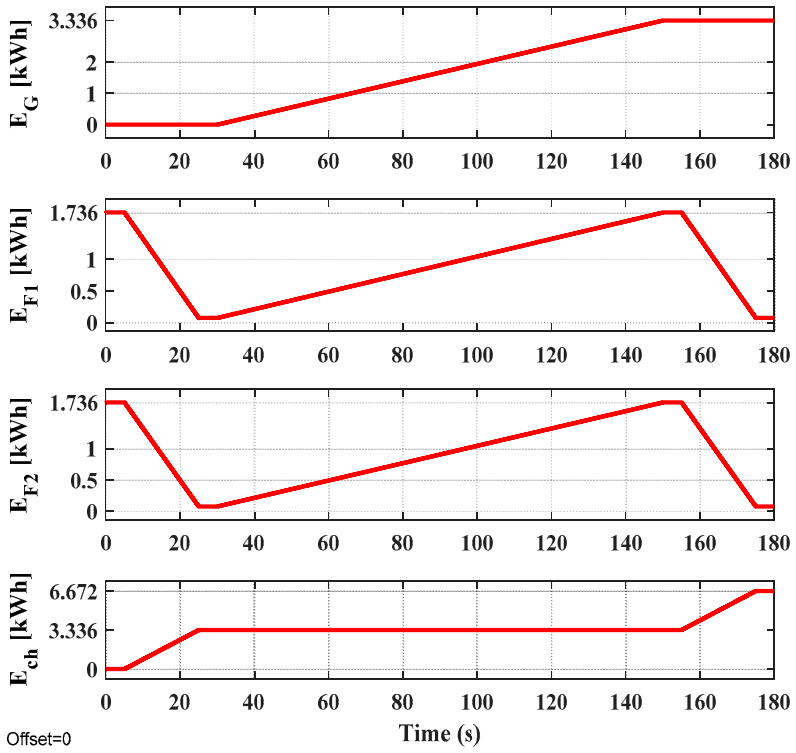


Figure 18. Simulation results for the electric energy of grid, FES1, FES2, and charger.

6. Experimental Results

In this section, an experimental setup for FESS with a power of 2.4 kW with the specifications shown in Table 6 was used. To control FESS, the DSP TMS320F28335 was used. Additionally, to detect rotor speed and position, the Omron Encoder E6B2-CWZ6C with a resolution of 2000 pulses/rotation was used [28]. Further analyzes, control methods, simulation, and laboratory results are provided for this laboratory setup in [28].

According to the FESS specifications presented in Table 6, and considering the FESS minimum speed $\omega_{\min} = 0.1\ \omega_{max}$, the maximum energy of this FESS is obtained from the following equation:

$$E_{max} = \frac{1}{2} J(\omega_{max} - \omega_{\min})^2 = 6400 \text{ Ws} \quad (44)$$

Table 6. Parameter values of FESS.

Motor Specification			Fundamental Specification		
Parameter	***Unit***	***Value***	**Parameter**	***Unit***	***Value***
L_{ds}	mH	55	Rated Power	kW	2.4
L_{qs}	mH	23	Rated Speed	rpm	6000
J	kg·m^2	0.04	Phase voltage	V	380
r_s	Ω	3.5	Phase current	A	9
p	-	4	Power factor	-	0.78
λ	wb	0.1			
K_f	wb	0.0001			

According to the rated power of FESS ($P_n = 2.4$ kW), the maximum time that FESS can charge the load (electric bus battery emulator) is obtained from the following equation:

$$\Delta t_{max} = \frac{E_{max}}{P_n} = \frac{6400 \text{ Ws}}{2400 \text{ W}} = 2.66 \text{ s} \tag{45}$$

According to the above results, FESS specifications for laboratory testing are considered in Table 7. Figure 19 shows the laboratory stand for the proposed charging station. Here, two switches were used to create the mode of disconnecting and connecting the electric bus load emulator. When the load is connected to the station (in other words, the electric bus is connected to the charging station for charging), the switch $S1$ is in the off position and the switch $S2$ is in the connected position. Additionally, when the load is disconnected from the station (there is no electric bus in the station for charging), the switch $S1$ is on and the switch $S2$ is off. Here, a resistance load was used to model the battery of an electric bus. The amount of resistance load according to the specifications presented in Table 7 is obtained from the following equation:

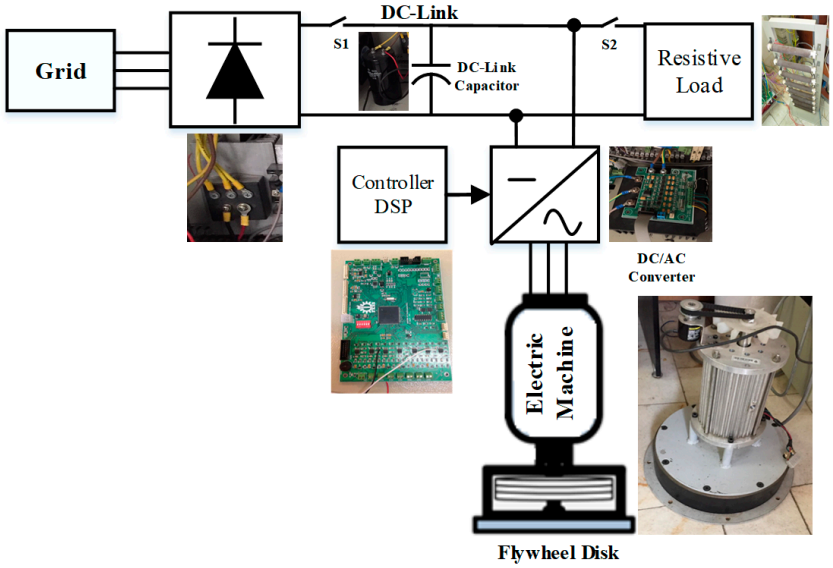
$$R = \frac{{V_{DC}}^2}{P_F} = 121 \ \ \Omega \tag{46}$$

Table 7. FESS laboratory setup specification.

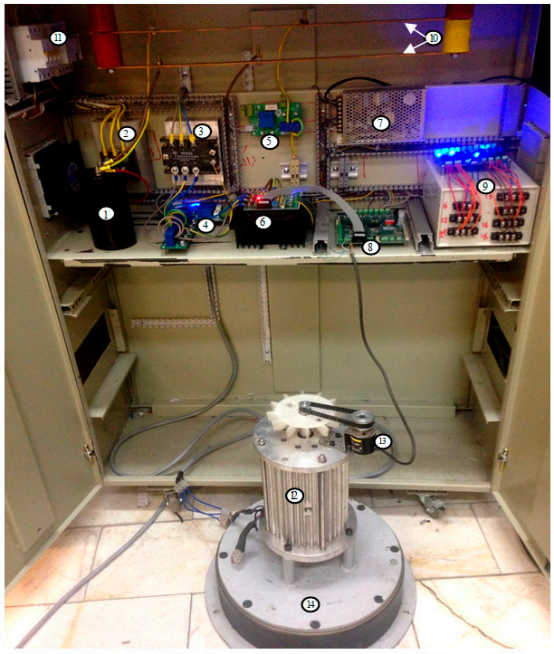
Parameters	Value
FESS rated power	$P_F = 2.4$ kW
FESS rated energy	$E_F = 6000$ Ws
DC link Voltage	$V_{DC} = \sqrt{2}\sqrt{3}\ V_{rms} = 538.88$ V
FESS discharging time	$\Delta t_{ch} = 2.5$ s
FESS charging time	$\Delta t_{rch} = 10$ s
Grid power to charge FESS	$P_G = 600$ W
Duration to connect S2 and disconnect S1	$\Delta t_C = 0.5$ s
Duration to connect S1 and disconnect S2	$\Delta t_d = 0.5$ s

Figure 20 shows the experimental results for the proposed flash charging structure. Figure 20a shows the FESS charge and discharge current. According to this figure, the current of the flywheel at the time of loading the load (electric bus battery emulator) in proportion to its nominal power is equal to 4.4 A and, at the time of recharging from the network, it is equal to 1.1 A in proportion to the charging power from the network. The FESS current is also zero during disconnection and connection times. According to

Figure 20b, the mains current is zero at the time of loading by the flywheel and 1.1 A at the time of FESS recharging in proportion to the power required by the network to recharge the FESS. As can be seen from Figure 20c, the load charging current in $\Delta t_{ch} = 2.5$ s corresponds to the charging power or rated power of FESS equal to 4.4 A. Figure 21 shows the DC bus voltage. According to this figure, the value of DC link voltage is equal to $V_{DC} = \sqrt{2}\sqrt{3}\ V_{rms} = 538.88$ V, but it fluctuates at the time of disconnection and connection of switches, and this perturbation is the criterion of FESS control to supply the required power to the load.



(**a**)



1- DC-Link Capacitor, 2- Three-Phase Diode Rectifier, 3- Solid State Relay (SSR), 4- AC Current and Voltage Sensor, 5- DC Current and Voltage Sensor, 6- IPM 3-Phase Inverter, 7- Switching Power Supply, 8- DSP Control Board, 9- Isolated Power Supply 10- DC-Link, 11- Protection Fuses, 12- Electric Machine, 13- Encoder, 14- Flywheel

(**b**)

Figure 19. Experimental setup: (**a**) laboratory setup schematic and (**b**) laboratory construction.

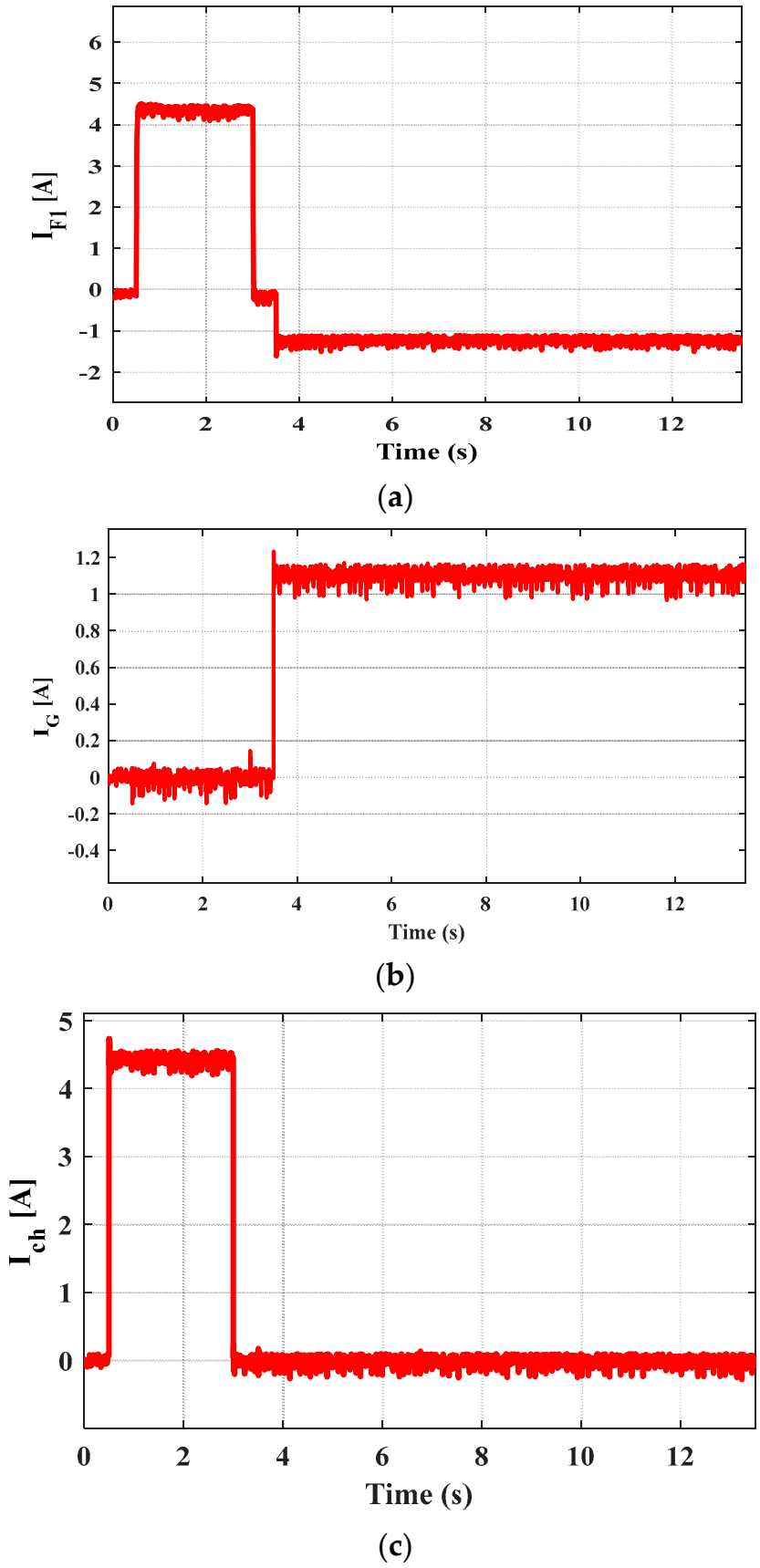


Figure 20. Experimental setup: (**a**) FESS current, (**b**) grid current, and (**c**) charger current.

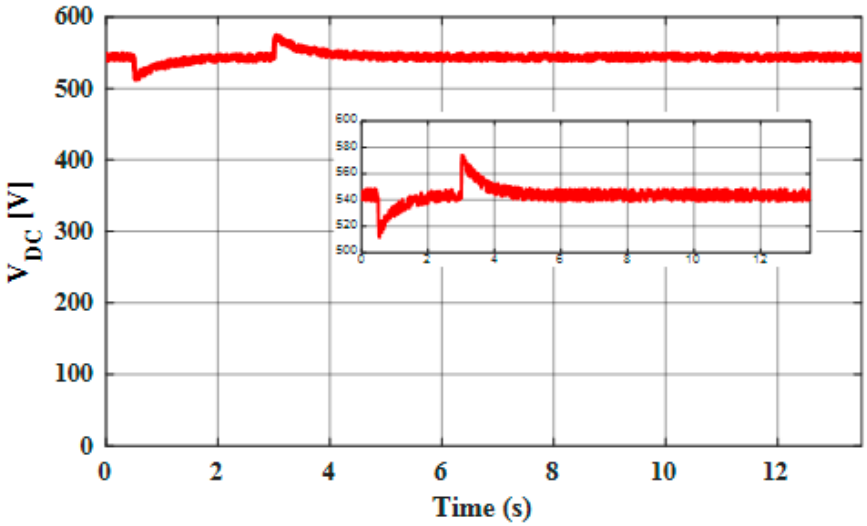


Figure 21. Experimental result for the DC-link voltage.

The experimental result for the FESS speed is shown in Figure 22. According to this figure, during FESS discharging, the speed decreases from the rated speed of 6000 rpm. When the charging cycle starts, the FESS is recharged and the speed of the rotating disk increases.

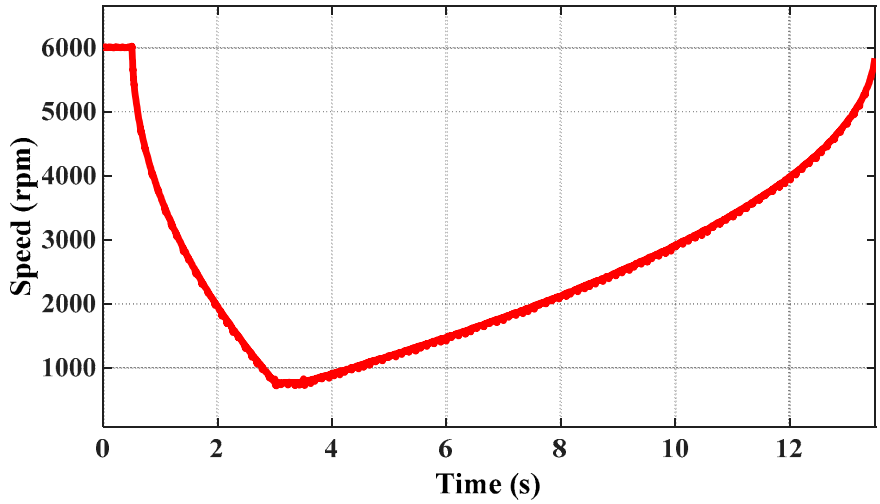


Figure 22. Experimental result for FESS speed.

7. Conclusions

In this paper, a FESS-based flash charging station was designed and sized. Based on the specifications of Tehran Line 1 BRT and the specifications of the electric bus (TOSA E-bus), 12 charging stations along the Line 1 should be installed. Each flash charging station has a charging energy capacity of 3.334 kWh with a power of 600 kW. These stations charge the battery of the electric buses for 20 s during stopping at the bus station. In the presence of these flash charging stations along the route of Tehran Line 1, any electric bus with a battery capacity of 80 kWh can be transporting passengers without any interruption. The components of the proposed flash charging station were electrically designed. Additionally, the important technical specifications of FESS and power electronic converters were extracted. Based on the economic comparison, the Levelized cost of electricity of FESS and lead-acid battery are 0.1983 EUR/kWh and 0.225 EUR/kWh, respectively. Annualized life cycle costs of FESS and lead-acid batteries are 495.77 EUR/kW-y and 580 EUR/kW-y, respectively. Additionally, the total capital cost of FESS and lead-acid batteries are 377 EUR/kWh and 2400 EUR/kWh, respectively. According to these results for economic calculations, the

proposed FESS-based flash charging station is more cost-effective in comparison with the conventional charging station based on lead-acid battery. In this paper, the charging strategy based on the charging duty cycle and FESS control method to control the charging and discharging of this system was presented. The simulation results proved the validity of the theoretical analysis. Additionally, to show the feasibility of the proposed structure, a small-scale laboratory setup was presented and its technical specifications were designed. The experimental results proved the effectiveness of the control method and the charging strategy. By using the proposed structure in Tehran line 1 BRT, it is possible to use electric buses despite the network limitations. The results of this work can be used in the transition from existing vehicles in the oil and gas industries to modern electric vehicles.

Author Contributions: Conceptualization, M.S.Z. and A.V.; methodology, M.S.Z. and H.A.M.; software, M.S.Z.; validation, M.S.Z., A.V. and H.A.M.; formal analysis, M.S.Z.; investigation, M.S.Z. and P.A.K.; resources, M.S.Z.; data curation, M.S.Z. and H.A.M.; writing—original draft preparation, M.S.Z.; writing—review and editing, M.S.Z., A.V. and P.A.K.; visualization, M.S.Z.; supervision, A.V.; project administration, M.S.Z.; funding acquisition, M.S.Z. All authors have read and agreed to the published version of the manuscript.

Funding: This research received no external funding.

Acknowledgments: The authors would like to thank the Ministry of Science and Higher Education of the Russian Federation within the framework of the development program of a world-class research center (agreement number 075-15-2022 -297) for supporting the publication of this paper in the Energies journal.

Conflicts of Interest: The authors declare no conflict of interest.

References

1. Pal, N.; Zhang, X.; Ali, M.; Mandal, A.; Hoteit, H. Carbon Dioxide Thickening: A Review of Technological Aspects, Advances and Challenges for Oilfield Application. *Fuel* **2022**, *315*, 122947. [CrossRef]
2. Ababneh, H.; Hameed, B.H. Electrofuels as Emerging New Green Alternative Fuel: A Review of Recent Literature. *Energy Convers. Manag.* **2022**, *254*, 115213. [CrossRef]
3. Khafizova, E. Specialized Transport Is an Integral Part of the Oil and Gas Industry//Special Equipment and Transport [Electronic Resource]. Available online: https://spec-technika.ru (accessed on 1 September 2022).
4. Su, W.; Eichi, H.; Zeng, W.; Chow, M.-Y. A Survey on the Electrification of Transportation in a Smart Grid Environment. *IEEE Trans. Ind. Inform.* **2011**, *8*, 1–10. [CrossRef]
5. Jiang, H.-D.; Xue, M.-M.; Liang, Q.-M.; Masui, T.; Ren, Z.-Y. How Do Demand-Side Policies Contribute to the Electrification and Decarburization of Private Transportation in China? A CGE-Based Analysis. *Technol. Forecast. Soc. Chang.* **2022**, *175*, 121322. [CrossRef]
6. Lajunen, A.; Kivekäs, K.; Vepsäläinen, J.; Tammi, K. Influence of increasing electrification of passenger vehicle fleet on carbon dioxide emissions in Finland. *Sustainability* **2020**, *12*, 5032. [CrossRef]
7. Ketelaer, T.; Kaschub, T.; Jochem PFichtner, W. The potential of carbon dioxide emission reductions in German commercial transport by electric vehicles. *Int. J. Environ. Sci. Technol.* **2014**, *11*, 2169–2184. [CrossRef]
8. Mao, F.; Li, Z.; Zhang, K. Carbon dioxide emissions estimation of conventional diesel buses electrification: A well-to-well analysis in Shenzhen, China. *J. Clean. Prod.* **2020**, *277*, 123048. [CrossRef]
9. Dickerman, L.; Harrison, J. The Electric Car Is Back (with Help from New Batteries, a Smarter Grid, and Uncle Sam). *IEEE Power Energy Mag.* **2011**, 19–25.
10. Shareef, H.; Islam, M.M.; Mohamed, A. A Review of the Stage-of-the-Art Charging Technologies, Placement Methodologies, and Impacts of Electric Vehicles. *Renew. Sustain. Energy Rev.* **2016**, *64*, 403–420. [CrossRef]
11. Aggeler, D.; Canales, F.; Zelaya, H.; La Parra, D.; Coccia, A.; Butcher, N.; Apeldoorn, O. Ultra-Fast DC-Charge Infrastructures for EV-Mobility and Future Smart Grids. In Proceedings of the 2010 IEEE PES Innovative Smart Grid Technologies Conference Europe (ISGT Europe), Gothenburg, Sweden, 11–13 October 2010; IEEE: Piscataway, NJ, USA, 2010; pp. 1–8.
12. Ideal Pantograph Charging Solution to Charge Fully Automated Electric Buses. ABB.com. Available online: https://global.abb/group/en/technology/did-you-know/pantograph-up-for-electric-bus (accessed on 10 September 2022).
13. Rubino, L.; Capasso, C.; Veneri, O. Review on Plug-in Electric Vehicle Charging Architectures Integrated with Distributed Energy Sources for Sustainable Mobility. *Appl. Energy* **2017**, *207*, 438–464. [CrossRef]
14. Heger, M.; Sarraf, M. Air Pollution in Tehran: Health Costs, Sources, and Policies. In *Environment and Natural Resources Global Practice Discussion Paper*; No. 6; World Bank: Washington, DC, USA, 2018. Available online: https://hdl.handle.net/10986/29909 (accessed on 10 September 2022).

15. Deng, J.; Shi, J.; Liu, Y.; Tang, Y. Application of a hybrid energy storage system in the fast charging station of electric vehicles. *IET Gener. Transm. Distrib.* **2016**, *10*, 1092–1097. [CrossRef]
16. Veneri, O.; Capasso, C.; Iannuzzi, D. Experimental evaluation of DC charging architecture for fully-electrified low-power two-wheeler. *Appl. Energy* **2016**, *162*, 1428–1438. [CrossRef]
17. Capasso, C.; Veneri, O. Experimental study of a DC charging station for full electric and plug in hybrid vehicles. *Appl. Energy* **2015**, *152*, 131–142. [CrossRef]
18. Ali, A.; Shakoor, R.; Raheem, A.; Muqeet, H.A.U.; Awais, Q.; Khan, A.A.; Jamil, M. Latest energy storage trends in multi-energy standalone electric vehicle charging stations: A comprehensive study. *Energies* **2022**, *15*, 4727. [CrossRef]
19. Pamuła, T.; Pamuła, W. Estimation of the Energy Consumption of Battery Electric Buses for Public Transport Networks Using Real-World Data and Deep Learning. *Energies* **2020**, *13*, 2340. [CrossRef]
20. Al-Ogaili, A.S.; Al-Shetwi, A.Q.; Al-Masri, H.M.K.; Babu, T.S.; Hoon, Y.; Alzaareer, K.; Babu, N.V.P. Review of the Estimation Methods of Energy Consumption for Battery Electric Buses. *Energies* **2021**, *14*, 7578. [CrossRef]
21. Luigi Lonoce, V.H. Bruce Warner, Grid Compatible Flash Charging Technology. In Proceedings of the 1st E-Mobility Power System Integration Symposium, Berlin, Germany, 24–27 October 2017.
22. De Filippo GMarano, V.; Sioshansi, R. Simulation of an electric transportation system at The Ohio State University. *Appl. Energy* **2014**, *113*, 1686–1691.
23. Amiryar, M.E.; Pullen, K.R. A review of flywheel energy storage system technologies and their applications. *Appl. Sci.* **2017**, *7*, 286. [CrossRef]
24. Mohamed, A.T. *Emerging Nanotechnology Applications in Electrical Engineering*; IGI Global: Hershey, PA, USA, 2021; p. 318.
25. Zakeri, B.; Syri, S. Electrical energy storage systems: A comparative life cycle cost analysis. *Renew. Sustain. Energy Rev.* **2015**, *42*, 569–596. [CrossRef]
26. Habibzadeh, M.; Mirimani, S.M. A Novel Implementation of SVM-DTC: Integrated Control of IPM Motor and Hybrid Energy Storage System for Electric Vehicle Application. *Iran. J. Electr. Electron. Eng.* **2021**, *17*, 1931.
27. Mendoza, A.; Argueta, J. *Performance Characterization-GM EV1 Panasonic Lead Acid Battery*; Southern California Edison: Rosemead, CA, USA, 2000.
28. Zarbil, M.S.; Vahedi, A.; Moghaddam, H.A.; Saeidi, M. Design and Implementation of Flywheel Energy Storage System Control with the Ability to Withstand Measurement Error. *J. Energy Storage* **2021**, *33*, 102047. [CrossRef]
29. Haidar, A.M.A.; Muttaqi, K.M.; Sutanto, D. Technical Challenges for Electric Power Industries Due to Grid-Integrated Electric Vehicles in Low Voltage Distributions: A Review. *Energy Convers. Manag.* **2014**, *86*, 689–700. [CrossRef]